Journal of Quantitative Spectroscopy & Radiative Transfer 182 (2016) 225–239

Contents lists available at ScienceDirect

Journal of Quantitative Spectroscopy & Radiative Transfer

journal homepage: www.elsevier.com/locate/jqsrt

Effects of surface roughness with two scales on light scattering by hexagonal ice crystals large compared to the wavelength: DDA results

C.T. Collier [a,*], E. Hesse [a], L. Taylor [a], Z. Ulanowski [a], A. Penttilä [b], T. Nousiainen [c]

[a] University of Hertfordshire, Centre for Atmospheric and Instrumentation Research, Hatfield, Hertfordshire AL10 9AB, UK
[b] Department of Physics, University of Helsinki, P.O. Box 64, FI-00014, Finland
[c] Finnish Meteorological Institute, FI-00101 Helsinki, Finland

ARTICLE INFO

Article history:
Received 10 February 2016
Received in revised form
5 June 2016
Accepted 6 June 2016
Available online 9 June 2016

Keywords:
Light scattering
Rough ice crystals
Cirrus
DDA

ABSTRACT

The effect of ice crystal surface roughness on light scattering by ice crystals which are large compared to the wavelength was studied, in particular changes to the 2D scattering patterns, azimuthally averaged phase functions, degree of linear polarisation patterns and asymmetry parameters for a range of orientations and roughness scales. It was found that roughness has an effect on light scattering by hexagonal prisms, particularly when the roughness features are of comparable size to the wavelength. The roughness model that has the most effect on light scattering takes account of more than one roughness scale.

Rough geometry was implemented by a Gaussian roughness method that took roughness parameters derived from sand grains, which have been reported to be suitable proxies for rough ice crystals. Light scattering data for these geometries was computed using the ADDA discrete dipole approximation method.

1. Introduction

A hospitable climate is vital to our long-term survival, and so the study of it is very important. The conclusion that the climate is being changed rapidly by human activity [1] makes this study even more urgent. Future climate behaviour can be predicted by the use of climate models, which work well for predicting the global climate decades into the future; however, there are necessarily assumptions and simplifications involved that limit the accuracy of these methods. One of the largest sources of error within these models is the interaction of clouds with radiation [2]. It is known that clouds have a large effect [3–5], but their interaction with climate is complex; their overall effect depends on the balance between reflected, absorbed and transmitted shortwave (from the sun) and longwave (from the surface and lower clouds) radiation [6].

Although cirrus clouds typically allow most incident sunlight to pass through them, their extent makes them a major factor for the climate; cirrus coverage is typically 30% [7]; over the tropics it is typically 70% [8]. It has been shown that smooth hexagonal prisms with size parameter $X = 2\pi r/\lambda$ (where r is the characteristic length of the particle and λ is the wavelength of the incident light) of at least 100 exhibit the 22° halo [9]. This minimum size is a consequence of diffraction – if the ice crystals are too small then diffraction effects become stronger and the halo peak is spread out. The halo is quite rarely seen with real cirrus clouds [9] potentially due to the constituent ice crystals in cirrus having complex geometries [10] and/or displaying

* Corresponding author.
E-mail addresses: ctcollier@gmail.com (C.T. Collier), e.hesse@herts.ac.uk (E. Hesse), l.taylor3@herts.ac.uk (L. Taylor), z.ulanowski@herts.ac.uk (Z. Ulanowski), antti.i.penttila@helsinki.fi (A. Penttilä), timo.nousiainen@fmi.fi (T. Nousiainen).

http://dx.doi.org/10.1016/j.jqsrt.2016.06.007
0022-4073/

surface roughness [11,12]; it is the latter which is the focus of this work. Note that it has also been reported in the literature [13] that irregularities in the geometry of hexagonal ice crystals can give rise to scattering properties indicative of surface roughness, such as the smoothing out of the phase function. Roughness of ice crystal surfaces has a large effect on the radiative properties – experimental results [14] show that surface roughness causes more light to be scattered in the backward hemisphere, lowering the asymmetry parameter. Understanding the extent to which roughness causes this effect is important for better characterising ice crystals in clouds.

Since direct imaging of particles in clouds is not accurate enough to characterise particle roughness [15], previous work on characterising ice crystal roughness has been done in the laboratory. Examples include using ice crystal analogues [14], studying ice growth under a scanning electron microscope [16–18], ice crystal creation using cloud chambers [19] and retrieval of roughness parameters from observations of dust [20]. Geometric optics has been used to simulate light scattering by particles with large-scale irregularity [21], in which deviations from perfect crystal geometry are modelled by randomly tilted facets. This method has also been applied to model surface roughness. However, as tilted facets are not usable within exact light scattering models, the simulation is not exactly repeatable and it does not account for more complex ray paths, as the tilting only occurs when the ray hits (i.e. there are no closed surfaces). Also, geometric optics is an invalid approximation at smaller size parameters and for wavelength-scale surface roughness features on larger size parameter objects. Improved roughness modelling has already been done, using the Improved Geometric Optics (for large size parameters) and Pseudospectral Time-Domain (for small size parameters) methods; however the parameters used there were not derived from physical

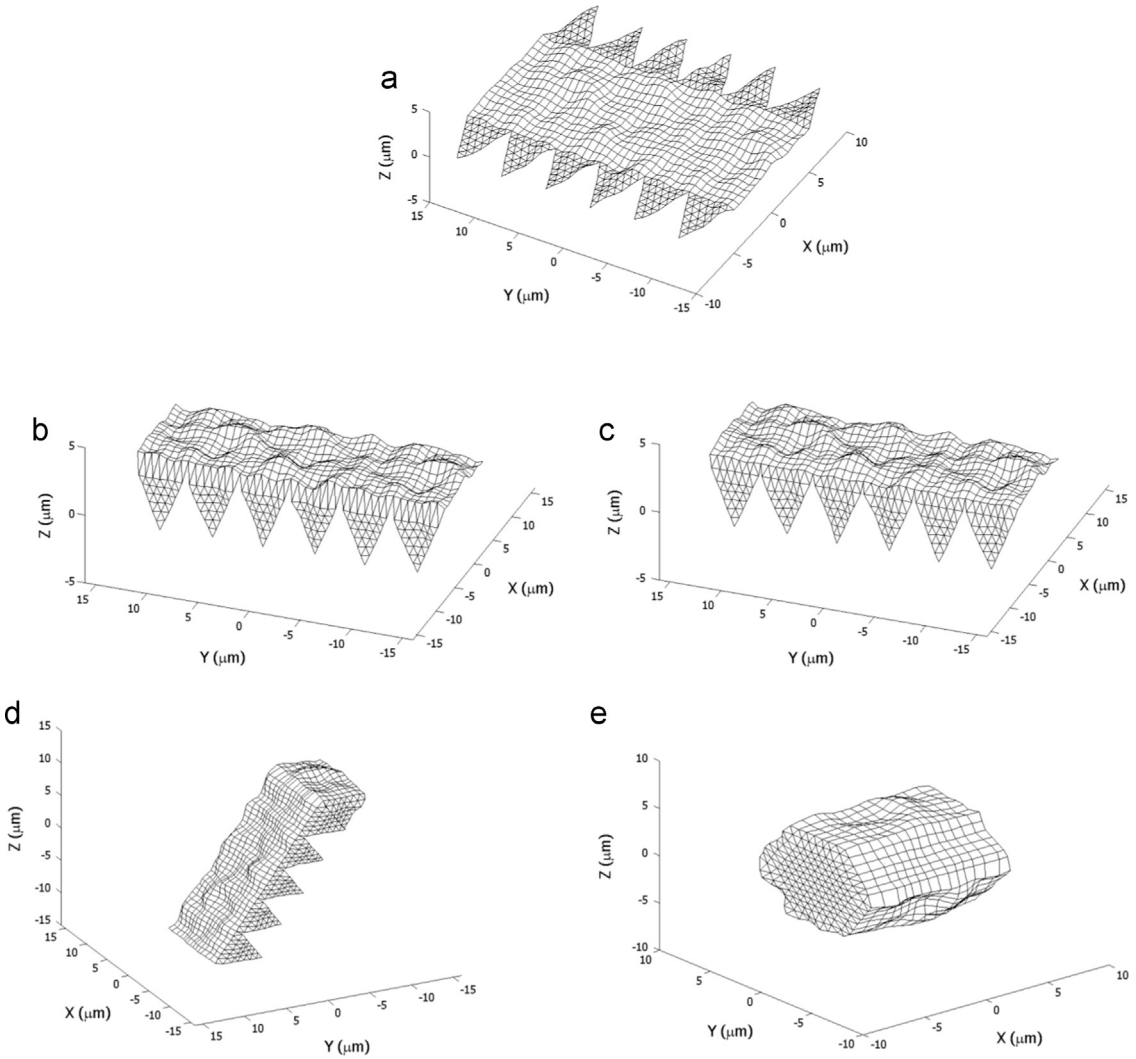

Fig. 1. (a) The crystal in its unfolded state. The triangles will be folded down, and then the rectangle will be folded to create the prism facets. (b) The crystal with its triangular parent facets folded down. Subfacet stretching can be seen at the edge where the rotation has taken place. (c) The crystal with its triangular parent facets folded down and corrected edge subfacets. (d) The crystal after one subfacet rotation is complete. (e) The crystal with all the sections folded into position and the unconnected edges joined together. (a)–(e) All have a correlation length of 1 μm and a standard deviation of 0.3 μm.

measurements and do not account for the possibility of multiple roughness scales [22].

In this work, Gaussian rough ice crystal models are created using parameters taken from analysis of sand grain surfaces, which have been found to have a similar effect on light scattering as ice crystal roughness [23]. Simulations were run using these roughened crystals on the Discrete Dipole Approximation (DDA) light scattering software ADDA [24].

2. Gaussian rough ice crystals

A Gaussian random crystal (Fig. 1e) is constructed from a Gaussian random surface (Fig. 1a). This is a surface for which the height varies as a function of the lateral x and y dimension; the height of each point is calculated as a Fourier series given in Eq. (1). Gaussian roughness has previously been used to describe roughness for cylinders [25], spheres [26], spheroids [27] and surfaces [28]. The fundamental parameters in Gaussian roughness are a correlation length, which describes the dominant spatial frequencies, and a standard deviation, which describes the variation in height.

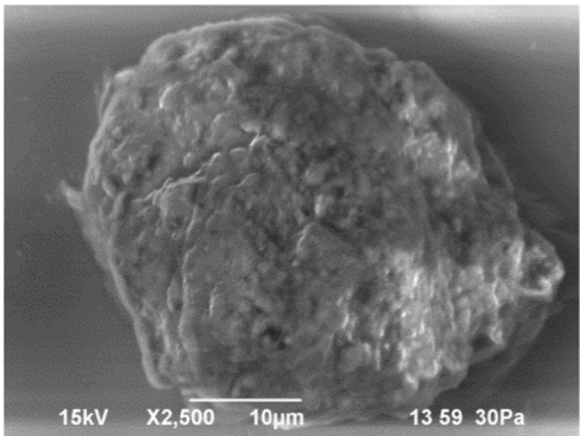

Fig. 2. An SEM scan of one of the analysed sand grains from Mitribah, Kuwait. It has a diameter of approximately 40 μm.

2.1. Gaussian random surface

A method was devised for creating input files describing the geometry of roughened hexagonal prisms for use with computational light scattering models.

The implementation of this involved the application of a Gaussian random surface creation method, adapted from previous work by Muinonen and Saarinen [25], which uses a 2D Fourier series technique, taking as its parameters the correlation length (l) and standard deviation of the height (σ) to create roughness across a previously flat surface. These two parameters can be chosen by the user; in this work they are determined from analysis of a sand grain. Theoretically, the height z of a point with coordinates (x,y) on a rough surface is given by the following:

$$z(x,y) = \sum_{p=-\infty}^{\infty} \sum_{q=-\infty}^{\infty} z_{pq}\, e^{i(pKx+qKy)} \tag{1}$$

Where $K=\pi/L$ is the wavenumber; L is half a period in x and y, and must be chosen to be large compared to the correlation length. z_{pq} are independent Gaussian random complex numbers, with zero means and variances:

$$Var(Re(z_{pq})) = \frac{1}{8}(1+\delta_{p0}+\delta_{q0}+5\delta_{p0}\delta_{q0})c_{pq}\sigma^2 \tag{2a}$$

$$Var(Im(z_{pq})) = \frac{1}{8}(1+\delta_{p0}+\delta_{q0}-3\delta_{p0}\delta_{q0})c_{pq}\sigma^2 \tag{2b}$$

The same z_{pq} values are used for all x,y. The c_{pq} are cosine series coefficients:

$$c_{pq} = \left[(2-\delta_{p0})\sqrt{\frac{\pi}{2}}\frac{l}{L}e^{-\left(\frac{1}{2}p^2\pi^2\frac{l^2}{L^2}\right)}\right]\left[(2-\delta_{q0})\sqrt{\frac{\pi}{2}}\frac{l}{L}e^{-\left(\frac{1}{2}q^2\pi^2\frac{l^2}{L^2}\right)}\right] \tag{3}$$

Practicality requires that the summations in Eq. (1) must be performed over finite ranges. As such, the correlation statistics of the surface must be taken into account to calculate suitable limits for p and q. To do this, we consider the correlation function representing a Gaussian random surface:

$$C(\zeta,\eta) = e^{-\left(\frac{\zeta^2+\eta^2}{2l^2}\right)} \tag{4}$$

Where ζ is the difference between the x positions of two points and η is the difference between the y positions of the same two points. The two dimensional Fourier

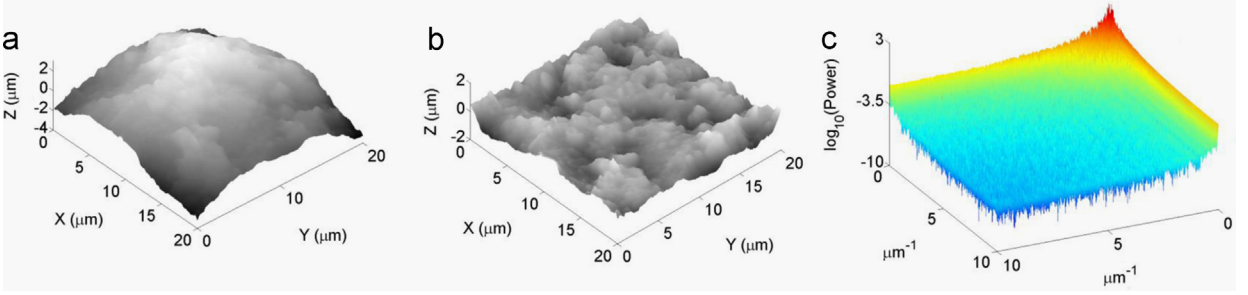

Fig. 3. (a) The surface before it has had the overall profile removed. (b) The surface after the overall profile has been removed. (c) Power spectrum of the surface in (b).

expansion of the surface correlation function is:

$$C(\zeta,\eta) = \sum_{p=-0}^{\infty}\sum_{q=-0}^{\infty} c_{pq}\cos pK\zeta\cos qK\eta \tag{5}$$

Evaluating Eqs. (4) and (5) for $\zeta=0$, $\eta=0$, we find the limits of the summations by seeking the p and q such that the difference between the two equations is less than 10^{-6}, that is:

$$1-\sum_{p=-p_0}^{p_{max}}\sum_{q=-q_0}^{q_{max}} c_{pq} < 1\times 10^{-6} \tag{6}$$

Where q_{max} must be less than or equal to p_{max}. Once p_{max} and q_{max} have been found, they can be substituted for the infinities in Eq. (1), which can be used to create the Gaussian random surface.

2.2. Crystal geometry creation

The process of creating a Gaussian random surface is shown in Fig. 1. The Gaussian random hexagonal prism is created by generating a roughened surface that can be folded to form a crystal. This is made up of six adjacent rectangular parent facets which form the prismatic facets and twelve equilateral triangular parent facets – two per prism facet – which eventually form the basal facets (Fig. 1a). After the roughening has been completed quadrilateral subfacets are generated.

Each triangular parent facet is folded along the edge between it and its adjoining prism facet, leaving them pointing down (Fig. 1b). It can be seen that subfacet stretching occurs where the triangular parents join the prism facets because the edge itself has not been rotated; to correct for this, the edge is rotated around its position in the unroughened state by 45° (Fig. 1c). Afterwards, the individual prism facets are rotated in turn (Fig. 1d).

Once the rotations are complete, gaps left due to the roughening procedure are joined together. The first and last prism facets are connected using an interpolation method. Likewise, interpolation is used to join the triangles at either end of the prism facets together to create the basal facets (Fig. 1e).

2.3. Obtaining Gaussian random surface parameters from sand grain microscopy

To obtain suitable parameters for roughness generation, analysis of the surface of an ice crystal in a cirrus cloud would be ideal. However, in situ cloud imaging methods are not able to provide the required optical resolution, and so a suitable proxy is needed. A sensitivity study using arbitrarily chosen roughness parameters would be the best approach; however the computational demands are prohibitive. An alternative technique is to derive roughness parameters from a physical model that shows similar levels of roughness to that of ice crystals;

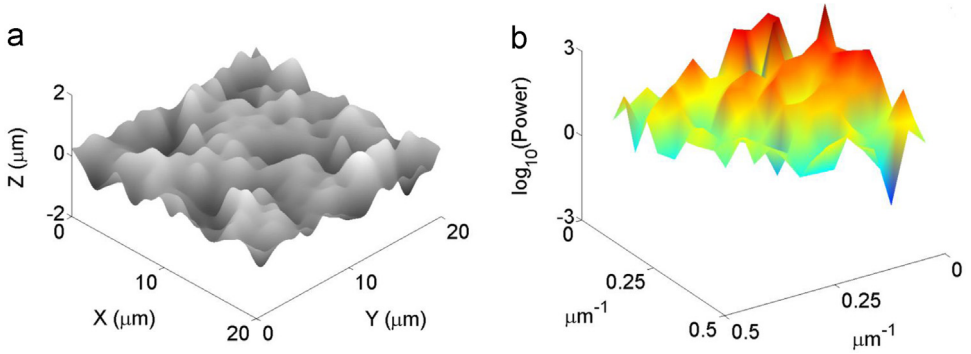

Fig. 4. (a) Simulated surface obtained after removing wavenumbers larger than 0.47 μm^{-1} from the Fourier transform of the surface in Fig. 3b and transforming back into spatial coordinates. (b) Power spectrum of the surface in (a).

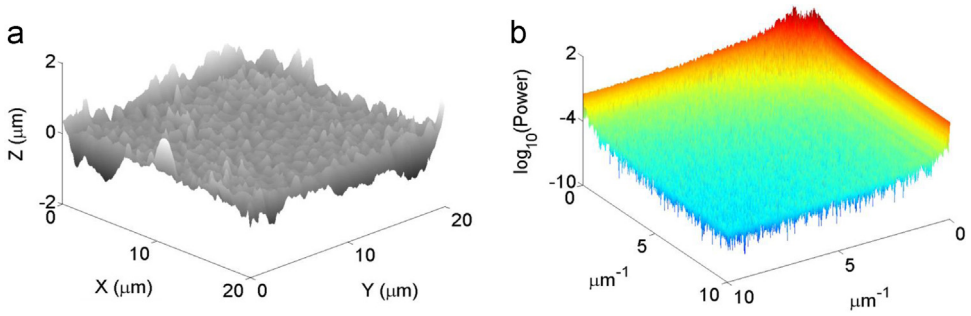

Fig. 5. (a) Simulated surface obtained after removing wavenumbers smaller than 0.47 μm^{-1} from the Fourier transform of the surface in Fig. 3b and transforming back into spatial coordinates. (b) Power spectrum of the surface in (a).

this is the method used in this study, which takes sand grains as the physical model. These were chosen because statistical measures of the texture of 2D scattering patterns taken by the SID-3 (Small Ice Detector) probe are consistent between sand grains and ice crystals from cirrus clouds [23].

Samples (e.g. Fig. 2) were prepared for detailed microscopy work using the Park Systems XE-100 Atomic Force Microscope (AFM) at Cardiff University. For this, suitably sized sand grains from a surface sample collected in Mitribah, Kuwait were selected using optical microscopy and mounted on a substrate. They needed to be less than approximately 50 μm in diameter, preferably close to this bound to get as large a scan area as possible (measured grains varied from 40 μm to 54 μm). Ulanowski et al. [23] showed that sand grains of diameter 41 μm and 47 μm display comparable scattering pattern-derived roughness to that of naturally occurring cirrus ice

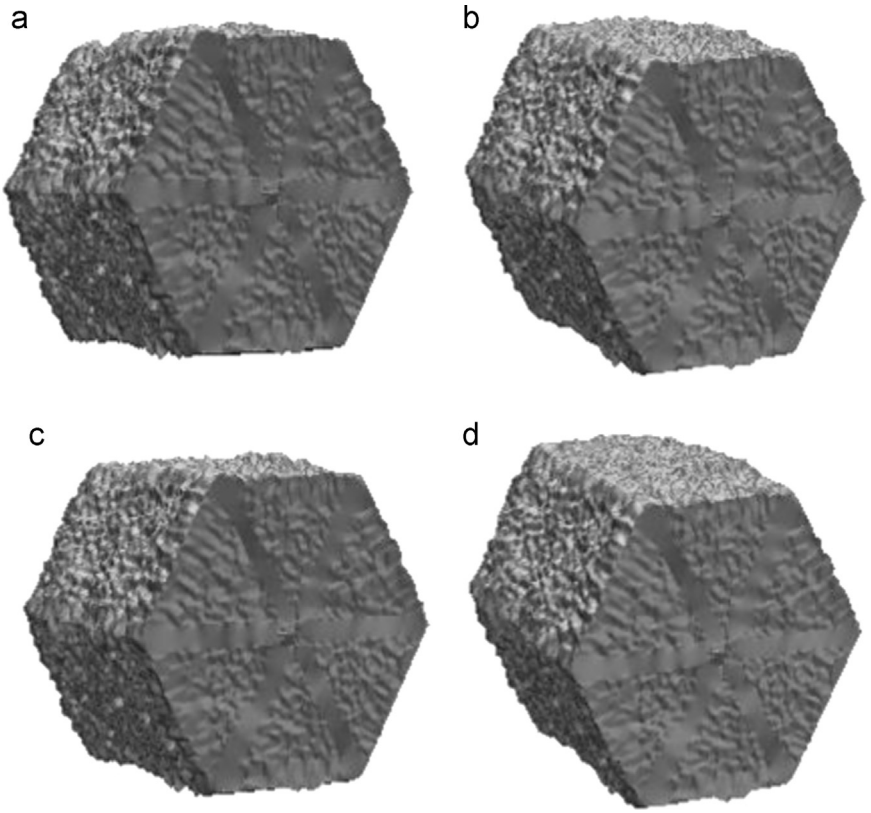

Fig. 6. The crystal orientations used in this work with the incident beam propagating out of the page, shown for a two-scale rough crystal. The stripes on the basal facets are a result of the interpolation used in the crystal creation procedure. All beam rotations are at 30° in the *x*–*y* plane; (a) has no other rotation, (b) is rotated 10° in the *y*–*z* plane, (c) is rotated 20° in the *y*–*z* plane and (d) is rotated 30° in the *y*–*z* plane. The coordinate system used can be seen in Fig. 7.

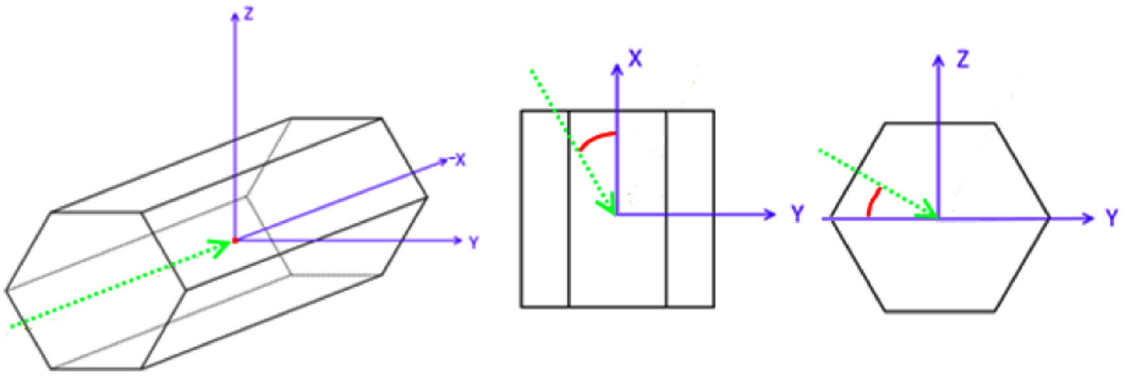

Fig. 7. Left: coordinate system of the incidence direction, which propagates in the negative *x* direction. Middle: the first rotation of the beam, which is around the *z*-axis. Right: the second rotation of the beam, which is around the *x*-axis.

crystals; similarly sized grains were chosen for this work because it is not known if this conclusion holds true at other sizes. This allowed for an effective scanning area of 20 μm × 20 μm, as the AFM probe is unable to scan areas that excessively deviate from being perpendicular to it.

To support the AFM work, images were taken of the topography of the sample grains using a Scanning Electron Microscope (SEM).

Data gained from the AFM work on sand grains was analysed to derive the correlation length and standard deviation values. Scanning artefacts were averaged out and the surface had a 2D polynomial subtracted from it to remove the grain's overall long-range profile and leave just the roughness (Fig. 3b). The 2D polynomial was calculated by performing a least square fit of the polynomial-generated surface to the measured surface; the order was increased until the roughness of the points of the resultant surface visually appeared to have no variation as a function of distance from the centre.

The resulting surface (Fig. 3b) was analysed to obtain correlation length and standard deviation values for the one-scale surface (as described in the next paragraph), before being Fourier transformed. A wavenumber cut-off was isotropically applied to split the power spectrum into two parts; one containing only the high spatial frequencies and one containing only the low spatial frequencies. Both of these were then transformed back into spatial coordinates to create two new surfaces. The one containing only low spatial frequencies was visually compared with the surface in Fig. 3b to check how it fit the latter's large scale features. The cut-off was varied until it satisfied this check. The resultant surfaces are shown in Figs. 4a and 5a with corresponding power spectra in Figs. 4b and 5b.

These surfaces were analysed to obtain values for the standard deviation and correlation length. Correlation lengths for both surfaces were retrieved by calculating autocorrelation and using a rearranged form of Eq. (4). The surface created using only large wavenumbers shows anomalously deviating z-values at the edges (a consequence of applying an isotropic cropping and therefore disregarding the effects of the finite sample size in the power spectrum), as can be seen in Fig. 5a. These were cropped out before the surface was used to derive these parameters. The same procedure was used to obtain correlation length and standard deviation for one-scale roughness by applying it to the surface containing all spatial frequencies (Fig. 3b). The correlation lengths and standard deviations derived from the surfaces in Fig. 3b, Figs. 4a and 5a were substituted into Eqs. (4) and (2), respectively. This allowed for the creation of a one-scale and a two-scale rough surface, both similar to that shown in Fig. 1a, to be created through using Eq. (1). By folding the resulting surface one is able to create a rough crystal; to obtain the two-scale rough crystal, the two rough surfaces are superimposed before folding. In effect, this method allows for the creation of rough particles with roughness properties derived from actual rough particles.

3. DDA results

Computations were carried out using the ADDA [24] implementation of the discrete dipole approximation light scattering method to find the light intensity and degree of linear polarisation (DLP, defined as $-P_{12}/P_{11}$, where these are both elements of the 4×4 scattering matrix) as a function of scattering angle and azimuthal angle for smooth, one-scale rough and two-scale rough hexagonal columns with an aspect ratio of 1 at a wavelength of 532 nm and refractive index $n=1.31+0.0i$. This aspect ratio was chosen since our main interest is in the effect of roughness, we note that this is in line with other studies, e.g. [13,22,29]. Four different directions of the incident beam were considered (Fig. 6) for a fixed crystal orientation (Fig. 7).

Using this model, the incident beam originally propagates along the x-axis; Fig. 7 shows the rotations performed to achieve these beam orientations; all make an angle of 30° with the x axis in the x–y plane, and make a final rotation of 0°, 10°, 20° or 30° around the x axis in the y–z plane projection. Four crystal size parameters were considered; 20, 40, 60 and 100, with roughness being scaled proportionately with size.

The number of dipoles in the DDA presentation of the geometry was chosen so that it can present the particle roughness with reasonable accuracy, and that the dipole size compared to the wavelength is small enough. For the latter requirement, the 'rule-of-thumb' for ADDA [24] is used, requiring that $d\leq 10/(\lambda|n|)$, with d being the dipole size. We selected $d=0.0406107$ for the largest size, so that dipoles-per-wavelength is 13.3, while smaller sizes are achieved by decreasing the dipole size.

There are no analytical methods to estimate the accuracy of our DDA results, but we can check how well they satisfy the reciprocity relation. Following the method in Schmidt et al. [30], we report the 90° relative reciprocity error to be 0.037% and 0.045% for the largest smooth geometry with VV- and HH-polarizations, and 0.0017% and 0.093% for the largest geometry with two-scale roughness and VV- or HH-polarizations. The relative reciprocity errors for these largest geometries are very small, and are expected to stay as small or get smaller with smaller geometries.

Table 1
Ratios of correlation length and standard deviation to the wavelength of the incident beam for one-scale and two-scale roughness at size parameters: 20, 40, 60 and 100. For these sizes, the number of dipoles used per wavelength was 66.5, 33.25, 22.17 and 13.3 respectively. The wavelength is 532 nm.

	One-scale roughness		Two-scale roughness				
			1st roughness scale		2nd roughness scale		
X	l/λ	σ/λ	l/λ	σ/λ	l/λ	σ/λ	Total σ/λ
20	0.31	0.06	0.68	0.08	0.08	0.04	0.12
40	0.63	0.13	1.35	0.16	0.16	0.09	0.25
60	0.94	0.19	2.03	0.24	0.24	0.13	0.37
100	1.57	0.31	3.38	0.41	0.41	0.22	0.63

Crystals with the dust-derived standard deviation and correlation length are created at a size parameter of 32.5. For one-scale roughness, correlation length 0.5 μm and standard deviation 0.1 μm are used; for two-scale roughness, the Gaussian random surfaces from the large scale mode (correlation length 1.08 μm and standard deviation 0.13 μm) and from the small scale mode (correlation length 0.13 μm and standard deviation 0.07 μm) were superimposed. The coordinates that make up this crystal are then scaled linearly to derive the coordinates of crystals of size parameter 20, 40, 60 and 100.

Due to the scaling, the roughness parameter to wavelength ratios increase linearly with size parameter, as can be seen in Table 1. As these ratio values increase, the effect of the roughness on light scattering also increases, as can be seen for azimuthally averaged phase functions (which appear in Fig. 8 and which, for brevity, we will call phase functions from here on), asymmetry parameters (Table 2), 2D scattering patterns (Figs. 11a and 12a) and degree of linear polarisation (Figs. 11–13). The Fraunhofer criterion [38] for effectively smooth surfaces requires $\sigma/\lambda < 1/(32\cos(\alpha))$ (corresponding to a phase difference of $\pi/8$

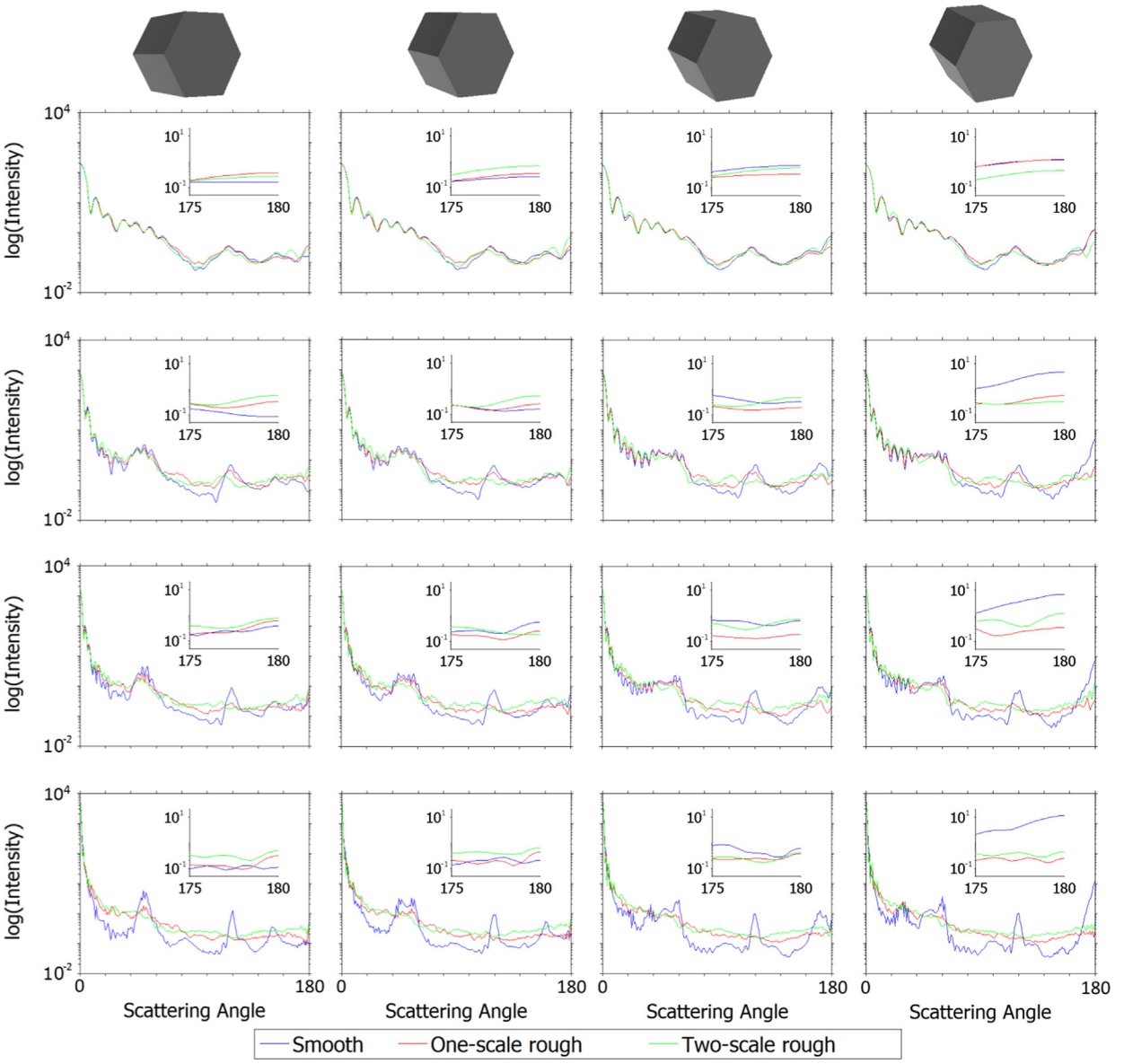

Fig. 8. Phase functions of smooth, one-scale rough and two-scale rough crystals. Different columns in the diagram represent different beam orientations – from left to right, the angle in the *y*–*z* plane increases from 0° to 30° in steps of 10°. Different rows represent different size parameters – from top to bottom, the size parameter is 20, 40, 60 and 100. Schematics above the top row show the crystal orientations where the incident beam propagates out of the page. Insets within the graphs show close-ups of the backscatter – from 175° to 180°. The same colours are used for the same roughness scales throughout the rest of this work. (For interpretation of the references to color in this figure legend, the reader is referred to the web version of this article.)

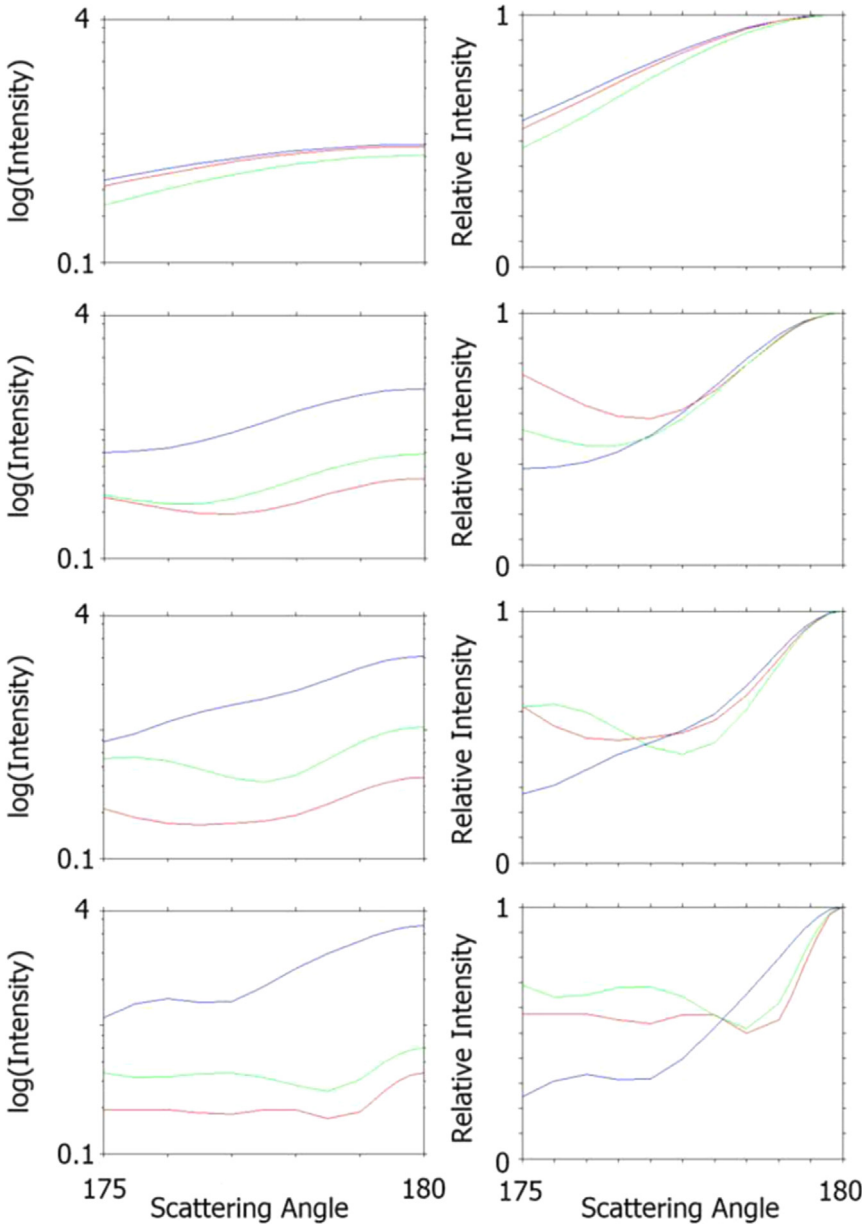

Fig. 9. 175°–180° phase functions for smooth (blue), one-scale rough (red) and two-scale rough (green) crystals averaged over all four orientations (left column) with corresponding "normalised-to-one" diagrams (right column). From top to bottom, the rows represent size parameters of 20, 40, 60 and 100. (For interpretation of the references to color in this figure legend, the reader is referred to the web version of this article.)

between two rays scattered at different points on the surface), where alpha is the angle between the incident wave vector and the surface normal of the corresponding smooth surface. For direct forward and backscattering the criterion has a value 0.031, which we note is about half the value for σ/λ for one scale roughness at size parameter 20, where the differences in scattering properties compared to the smooth crystal are found to be very small already.

Scattering from the largest size parameter smooth prism can be readily interpreted from a geometric/physical optics perspective, identifying peaks in the phase function as being caused by reflection/refraction events with local spreading caused by diffraction. We use the geometric optics terminology here as a means for interpreting the changes of scattering properties as the crystal is scaled. Light passing very close to the crystal is also scattered and so geometric optics (GO) ray tracing is usually combined with diffraction at the projected cross section (e.g. [21]), which we will refer to as external diffraction. If external diffraction is computed as diffraction at the incidence facing facets (a generalisation of Babinet's principle) and diffraction of rays or beams leaving the crystal is considered, scattering can be resolved azimuthally (e.g. [31,32]).

For the orientation with a rotation of 0° in the y–z plane, peaks can be seen for the smooth crystal at

scattering angles of 0° (transmission through the two parallel basal facets – known as δ-function transmission in GO [33] – superposed with the external diffraction peak), 51° (caused by reflection off the prism facets), 80° (due to light being transmitted through the two prism facets and passing through the two opposite them) and 120° (Figs. 11 and 12). This latter peak is mainly due to light reflecting off the basal facet and light passing through the basal facet facing the beam, internally reflecting off the other basal facet and exiting back through the first basal facet. There is also a peak at 151° due to at least two internal reflections either in one plane or including a rotation of reference plane (skew rays).

As the incident beam is rotated in the *x*–*y* plane, the prism reflection peak is split; at a rotation of 10°, peaks can be seen at scattering angles of 10°, 48°, 55°, 120° and 160°; at a rotation of 20°, peaks appear at scattering angles of 20°, 38°, 58°, 120° and 170°; finally, at a rotation of 30°, peaks are visible at scattering angles of 28°, 60°, 120° and 180° (see 4th row of Fig. 8, blue line). It is important to note that due to crystal symmetry more complex ray interactions can produce the same exit angle (e.g. external reflection and refraction into the crystal followed by internal reflection followed by refraction out of the crystal).

While such analysis is possible for smooth crystals, it becomes far more difficult when surface roughness is introduced due to the large number of sub-beams created at external incidence. Looking at the 2D scattering patterns in Figs. 11 and 12, we see that roughness reduces the prominent features seen for the smooth crystal into speckle. This blurring and spreading leads to the smoothing out of the peaks and troughs in the phase function (Fig. 8). For size parameter 100 the deviation in the phase function from the smooth case is substantial after a scattering angle of 10°. This can be seen also in the 2D scattering patterns by the external diffraction peak at the centre being the only remaining recognisable feature. Note that scattering in the direct forward direction is notably reduced due to roughness affecting the transmission peak, in particular for two-scale roughness (Table 3). Decreasing the size parameter reduces the influence roughness has on the 2D scattering patterns, with relatively little change occurring for the smallest size parameter (see Figs. 8 and 11). It can also be seen that two-scale roughness increases the number of speckle spots compared to one-scale, and that these spots decrease in size with increasing size parameter, as discussed in [34]. The scaling of roughness with size parameter means that smaller size parameters have roughness features which are much smaller than the wavelength (Table 1) which in turn means that light scattering is only weakly sensitive to it. If the roughness had not been scaled, it is possible that there would have existed surface roughness with size comparable to the wavelength. In such circumstances one would expect to observe a noticeable deviation from the smooth case in the associated scattering patterns and phase functions.

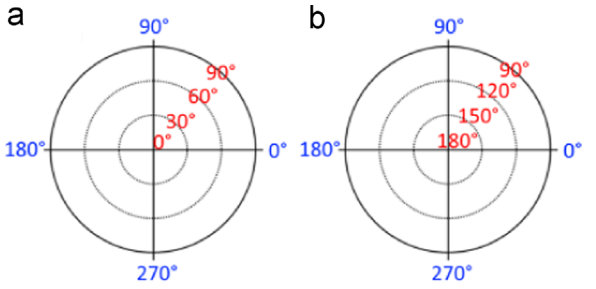

Fig. 10. Diagrams showing the azimuthal (blue) and scattering (red) angles for (a) forward 2D scattering patterns (Fig. 11) and backward 2D scattering patterns (Fig. 12). (For interpretation of the references to color in this figure legend, the reader is referred to the web version of this article.)

The 2D scattering patterns in Fig. 12 correspond to scattering in the backward hemisphere, where the effects of surface roughness are even more pronounced. For the largest size parameter, one can easily see that the bright spot at 120°, due to external reflection and some higher order events, is entirely removed as the reflection becomes diffuse and the transmission paths altered, leaving only speckle. Furthermore, we notice that surface roughness has less effect on the smallest size parameter, as for forward scattering.

In summary we see that deviations from the smooth case in the 2D scattering patterns and phase functions increase with size, and that forward scattering is less sensitive to

Table 2
Asymmetry parameters calculated for the crystals for which light scattering was modelled. The orientation angles refer to the rotations explained in Fig. 7.

Orientation	Smooth g_s	One-scale g_1	$\frac{(g_1-g_s)}{g_s}$[%]	Two-scale g_2	$\frac{(g_2-g_s)}{g_s}$[%]	Smooth g_s	One-scale g_1	$\frac{(g_1-g_s)}{g_s}$[%]	Two-scale g_2	$\frac{(g_2-g_s)}{g_s}$[%]
	Size parameter 20					Size parameter 40				
30°,0°	0.725	0.724	−0.207	0.744	2.607	0.710	0.694	−2.295	0.716	0.845
30°,10°	0.722	0.719	−0.471	0.740	2.535	0.700	0.689	−1.628	0.714	1.956
30°,20°	0.720	0.720	0.014	0.736	2.166	0.694	0.698	0.475	0.716	3.140
30°,30°	0.720	0.718	−0.292	0.734	2.043	0.698	0.705	1.046	0.723	3.583
Mean	0.722	0.720	−0.236	0.739	2.342	0.701	0.696	−0.628	0.717	2.354
	Size parameter 60					Size parameter 100				
30°,0°	0.711	0.722	1.434	0.702	−1.251	0.764	0.758	−0.785	0.726	−5.012
30°,10°	0.727	0.739	1.568	0.700	−3.713	0.761	0.758	−0.368	0.713	−6.280
30°,20°	0.725	0.738	1.779	0.710	−2.137	0.771	0.768	−0.389	0.724	−6.111
30°,30°	0.724	0.746	2.996	0.722	−0.373	0.766	0.767	0.170	0.729	−4.856
Mean	0.722	0.736	1.952	0.708	−1.883	0.766	0.763	−0.340	0.723	−5.577

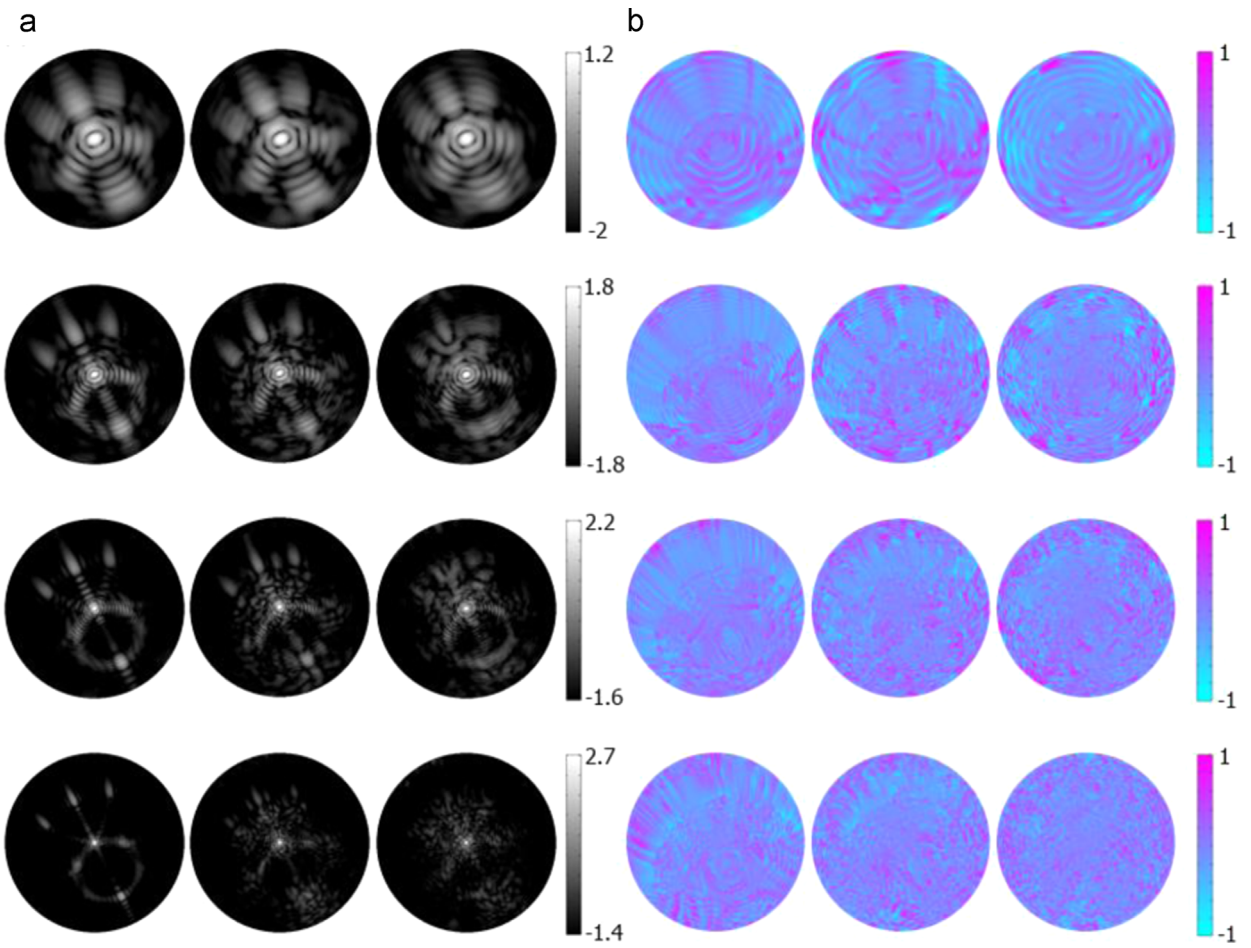

Fig. 11. Logarithmically scaled forward hemisphere 2D scattering patterns (a) and forward hemisphere degree of linear polarisation images (b) for the crystal shown in the inset of the 4th column of Fig. 8. Different rows represent different crystal size parameters; from top to bottom, they represent size parameters of 20, 40, 60 and 100. Different columns represent different roughnesses; from left to right they represent the smooth, one-scale rough and two-scale rough cases. The azimuthal (blue) and scattering (red) angles can be seen in Fig. 10(a). Since brightness increases with crystal size parameter, grey-scale ranges for the scattering patterns in (a) were varied to best show the features at each size parameter. (For interpretation of the references to color in this figure legend, the reader is referred to the web version of this article.)

surface roughness than back scattering. This is because external diffraction, which has low sensitivity to surface roughness as it depends on the crystal's 3-dimensional contour, strongly contributes to forward scattering. Furthermore, two-scale roughness results in more speckle than one-scale roughness because of the change in σ/λ which leads to considerable phase differences in the reflected light. Note that due to the scaling of roughness with size, σ/λ is greatest at larger size parameters, contributing to more pronounced speckle with increasing crystal size. However, the angular region enclosing the direct backscattering direction needs to be considered separately. For orientations where direct backscattering is strong for the smooth crystal due to retro-reflections at or close to 180° (4th column in Fig. 8) a reduction will be observed due to surface roughness, in a similar way as was discussed for other large angles. This effect is strongest for large size parameters and can be imagined as distortion of the GO ray paths. However, for orientations where direct backscattering is weak for the smooth crystal (first column in Fig. 8) a slight increase with surface roughness is seen, which would be predicted by GO due to suitable ray paths becoming available which could also contribute to coherent backscattering. Fig. 15 shows a 2D scattering pattern over the angular range $175^{\circ} \leq \theta \leq 180^{\circ}$ for the phase function for size parameter 100.

Surface roughness causes the scattered field to have a spatially wider distribution resulting in higher contributions into the direct backscattering direction. We expect there to be an 'optimum range' of roughness parameters which allows diffraction into the backscattering direction with sufficiently high electric field amplitude. The half-height width of the back scattering peak is about 0.6° for size parameter 100 and increases with decreasing crystal size. For size parameter 100 the phase functions between 175° and 180°of the two rough crystals look very similar for all four orientations. The absolute values for double scale roughness (see Figs. 8 and 15) are very slightly higher but the enhancement factor is slightly less than for single scale roughness. The latter is thought to be due to more spread out diffraction which results in smaller irradiance

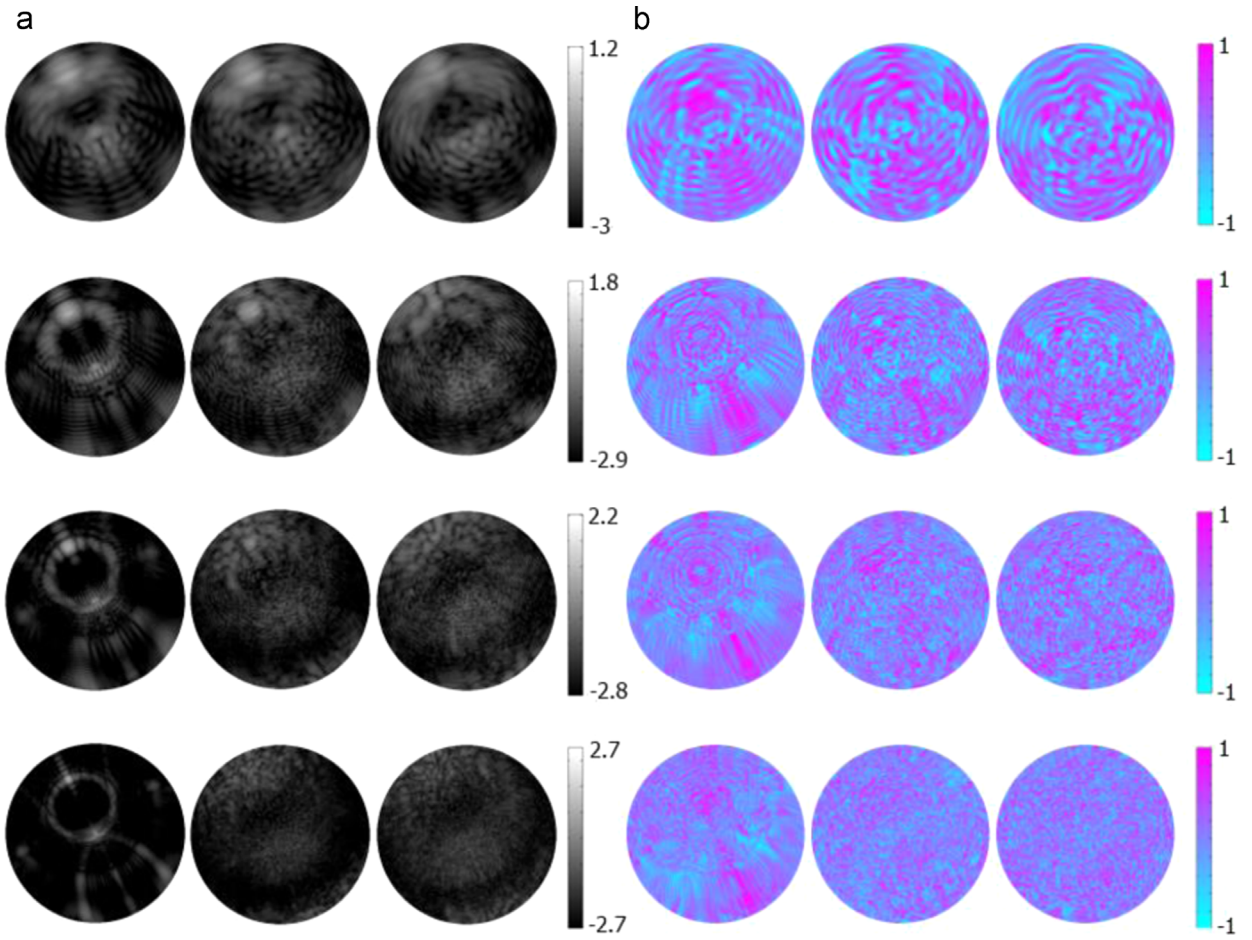

Fig. 12. Same as Fig. 11, but for the backward scattering hemisphere. The azimuthal (blue) and scattering (red) angles can be seen in Fig. 10(b). Notice that the size of the speckle in the 2D scattering patterns decreases with increasing size parameter. (For interpretation of the references to color in this figure legend, the reader is referred to the web version of this article.)

contributions to the backscattering peak. In this work the ratio of intensities at 180° and 175° is taken as a measure for backscattering amplification. For the roughened prisms, values averaged over the four orientations are 1.79 for the one-scale roughness and 1.45 for the two-scale. Note that the maximum possible enhancement factor due to interference is two. The observed peak height is fairly independent of particle size (see insets of Figs. 8 and 9). These observations are similar to results for roughened hexagonal crystals with random orientation in [29] and [35]. The effect of surface roughness on the polarisation of the scattered light for the cases investigated is best discussed through use of the right column of Fig. 13. These plots show clearly that the greatest deviation from the smooth crystal's polarisation occurs in the backscattering. This is no surprise since back-scattering is not only more sensitive to surface roughness, but also contains contributions from near spatial skew rays [36], which also change with surface roughness. For all but the smallest size parameter the magnitude of DLP stays broadly the same (away from backscattering), irrespective of roughness. Table 2 and Fig. 14 show the asymmetry parameters for several fixed orientations (which should not be considered to be representative of a cloud of randomly oriented ice crystals) derived from DDA, including percentages of deviation from the value for the smooth crystal. Crystal symmetry means that results for beam rotations of 0°, 10° and 20° around the *x*-axis apply to rotations around the same axis of 60°, 50° and 40°, respectively. Experimental results on ice analogues with submicron roughness (at size parameters of 395 and 493) [14] and modelling results using Improved Geometric Optics [37] have shown that the asymmetry parameter would be expected to be reduced for rough crystals compared to smooth ones. Modelling results from this study are in agreement with this, with the greatest reduction in the asymmetry parameter being seen at the largest size parameter with two-scale roughness, potentially indicating that the two-scale roughness is more representative of 'real' roughness.

4. Conclusions

2D scattering pattern, phase function, asymmetry parameter and degree of linear polarisation results were

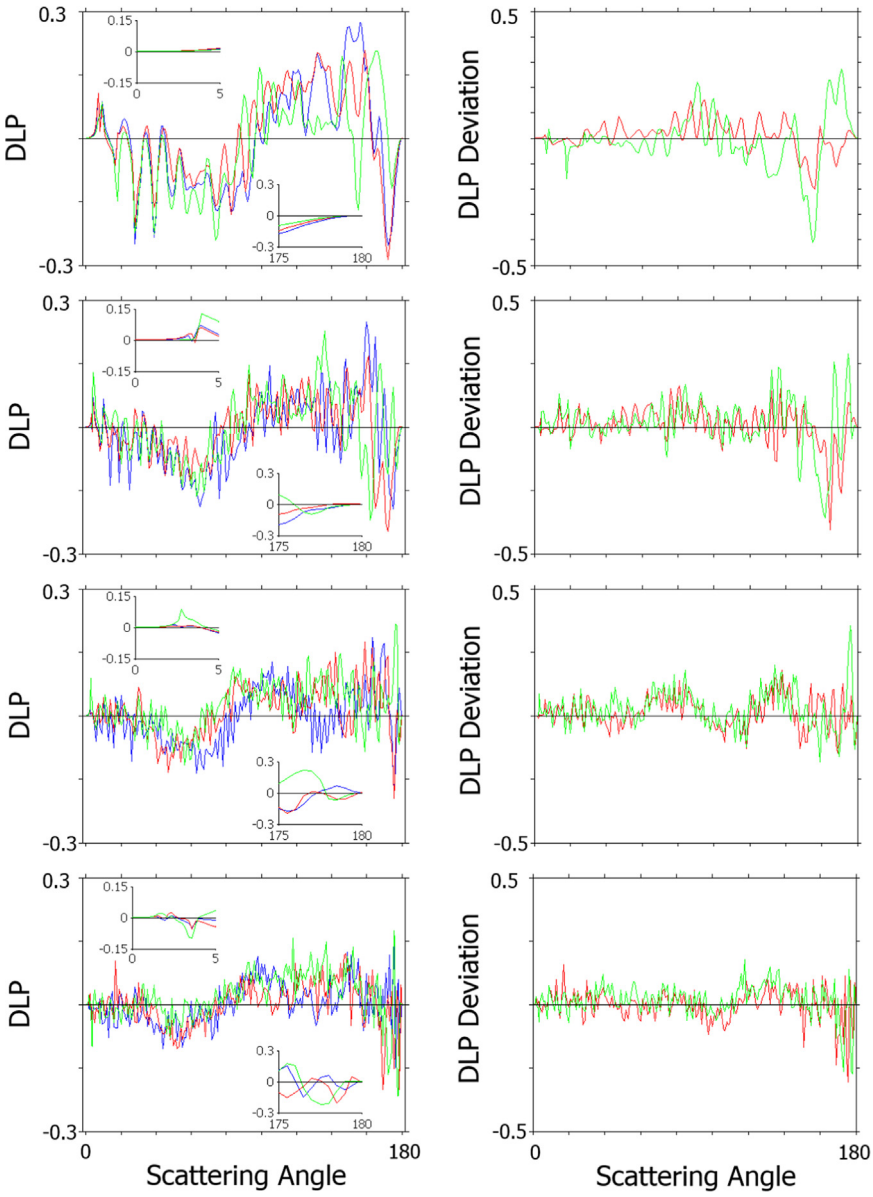

Fig. 13. Left column: azimuthally averaged degree of linear polarisation for smooth (blue), one-scale rough (red) and two-scale rough (green) crystals at the same orientation as in Figs. 11 and 12. The first and last 5 degrees can be seen in the insets. Right column: the difference between the DLP of the smooth crystal and the one-scale rough (red) and two-scale rough (green) crystals for each of the crystal sizes considered. The deviation graphs are intended to more clearly show where DLP for the rough crystals deviates from DLP for the smooth crystals. Different rows represent different crystal size parameters; from top to bottom, they represent size parameters of 20, 40, 60 and 100. (For interpretation of the references to color in this figure legend, the reader is referred to the web version of this article.)

computed using the ADDA code for smooth, one-scale and two-scale Gaussian rough crystals of various orientations and size parameters of 20, 40, 60 and 100. Fourier analysis of data obtained through atomic force microscopy of a grain of Kuwaiti desert sand returned correlation lengths and standard deviations which were used to create Gaussian rough surfaces. These rough surfaces were then folded to create rough crystals. The roughness was scaled linearly with crystal size.

2D scattering patterns for fixed orientation of known particle geometries are an important tool for interpreting SID-3 patterns. Our results show that roughness causes characteristic features related to smooth crystals to blur, fragment and disappear leaving behind speckle, when the scaling is large enough, for both forward and backward scattering hemispheres; the effect is strongest for the backscattering hemisphere. The roughness-induced deviations become more apparent as the crystal size parameter increases, and are more apparent for two-scale roughness than for one-scale roughness. With two-scale roughness at a size parameter of 100 considered, mainly the external diffraction peak with some speckle remains

Table 3
Percentage changes in direct forward transmission (i.e., a scattering angle of 0°) for one-scale and two-scale rough crystals, compared to the smooth crystal. The orientation angles refer to the rotations explained in Fig. 7.

Orientation	Size parameter 20		Size parameter 40		Size parameter 60		Size parameter 100	
	One-scale % change	Two-scale % change	One-scale % change	Two-scale % change	One-scale % change	Two-scale % change	One-scale % change	Two-scale % change
30°,0°	2.67	2.55	1.36	1.86	4.21	3.58	−2.36	−7.68
30°,10°	2.25	4.06	4.10	6.58	1.19	−0.39	−0.50	−5.36
30°,20°	2.20	3.28	4.52	9.45	0.95	−3.17	−2.64	−11.53
30°,30°	0.94	1.11	4.27	7.93	2.30	−2.14	−2.60	−12.80
Mean	2.02	2.76	3.53	6.37	2.12	−0.64	−2.05	−9.45

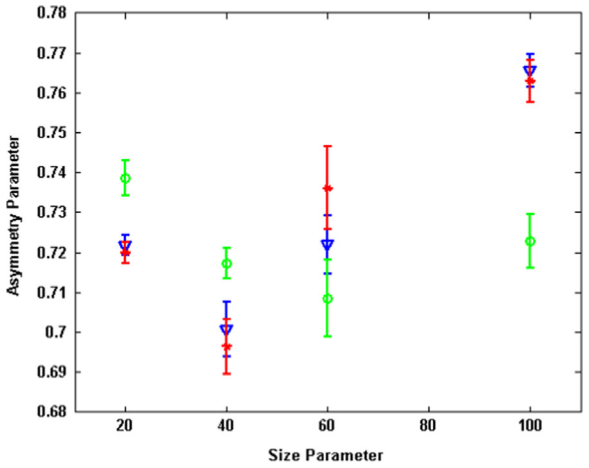

Fig. 14. Graphical representation of asymmetry parameter results of smooth (blue, triangle markers), one-scale rough (red, asterisk markers) and two-scale rough (green, circle markers) crystals. Markers show the position of the mean and bars show the standard deviation of the asymmetry parameter derived from the four computed orientations. Note that the orientations are not independent. (For interpretation of the references to color in this figure legend, the reader is referred to the web version of this article.)

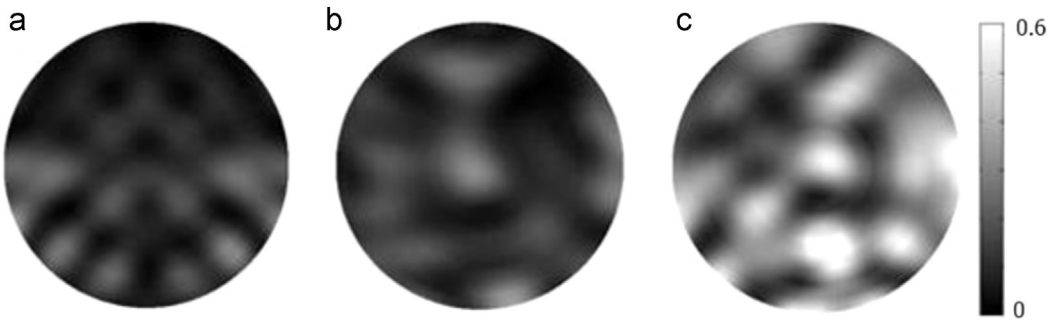

Fig. 15. Two-dimensional intensity patterns with linear scale for the size parameter 100 crystal in the orientation shown in the first column of Fig. 8 for the angular region $175^{\circ} \le \theta \le 180^{\circ}$. (a) corresponds to the smooth crystal, (b) the one-scale rough crystal and (c) the two-scale rough crystal. It can be seen that adding roughness increases the intensity of the backscattered light because of coherent backscattering.

for forward scattering. However, the angular region enclosing the direct backscattering direction needs to be considered separately. For orientations where direct backscattering is strong for the smooth crystal due to retro-reflections at or close to 180° it will be reduced by surface roughness in a similar way as discussed for other large scattering angles. Yet, for orientations where direct backscattering is weak for the smooth crystal it is slightly increased by surface roughness, which is thought to be partly due to coherent backscattering.

Phase functions show that the effects of roughness increase as the particle is scaled towards larger sizes with larger roughness features in the investigated range - little change is seen (compared to the smooth crystal case) for rough crystals scaled to a size parameter of 20. It should be noted that (l/λ) and (σ/λ) are very small at size parameter

20; wavelength scale roughness features may well increase light scattering by a crystal of this size.

As the asymmetry parameter is easily affected by orientation we cannot draw firm conclusions on how roughness affects it since the orientation sample is small. Calculation of a sufficient number of random orientations for proper orientation averaging would be extremely computationally expensive. That said, we see that deviation from the smooth case is largest when the two-scale roughness is used in conjunction with the largest size parameter, which is qualitatively in agreement with previous experimental results [14].

Degree of linear polarisation 2D patterns show that, compared to results for smooth crystals, roughness disrupts patterns in scattering angle and azimuth for forward and backward scattered light. Backward scattering is affected more than forward scattering; the same effect as seen for intensity. These effects become more pronounced as the crystal is scaled up in size and for two-scale roughness.

Overall we have shown that for hexagonal prisms Gaussian roughness with the investigated parameters reduces features seen in the phase function compared with the smooth counterpart and reduces the asymmetry parameter, as long as the effective period and amplitude of the spectrum of spatial oscillations making up the roughness are of an approximately equal or greater size to the wavelength – this appears to begin happening noticeably at a size parameter of 40. Larger roughness features cause more deviation from scattering observed for smooth crystals, but the most effective roughness model for ice crystals investigated here takes account of both large features and features whose size is small compared to the wavelength.

Acknowledgements

Many thanks are due to Emmanuel Brousseau of the Institute of Mechanical and Manufacturing Engineering at Cardiff University for his AFM work with sand grains. E Hesse and Z. Ulanowski acknowledge support by the Natural Environment Research Council (NERC), United Kingdom, grant NE/I020067/1. C.T. Collier and L. Taylor acknowledge support from the NERC Doctoral Training Programme. T. Nousiainen acknowledges funding by the Academy of Finland Grant no. 255718 and the Finnish Funding Agency for Technology and Innovation (Tekes) Grant no. 3155/31/2009. A. Penttilä acknowledges funding by the Academy of Finland Grant no. 1257966. The DDA results have been computed using CSC's resources. CSC is the Finnish IT Centre for Science and is owned by the Ministry of Education, Finland.

The authors also gratefully acknowledge the helpful contributions from two anonymous reviewers.

References

[1] Contribution of working group I to the fifth assessment report of the Intergovernmental Panel on Climate Change; 2013.
[2] Colman RA. A comparison of climate feedbacks in general circulation models. Clim Dyn 2003;20:865–73.
[3] Liou KN, Takano Y, Yang P Y. In: Mishchenko MI, Hovenier JW, Travis LD, editors. Light scattering by nonspherical particles. New York: Academic Press; 1999. p. 417–49.
[4] Baran AJ. From the single-scattering properties of ice crystals to climate prediction: A way forward. Atmos Res 2012;112:45–69.
[5] Yang P, Liou KN, Bi L, Liu C, Yi BQ, Baum BA. On the radiative properties of ice clouds: Light scattering, remote sensing and radiation parameterization. Adv Atmos Sci 2015;32(1):32–63.
[6] Wendisch M, Yang P, Pilewskie P. Effects of ice crystal habit on thermal infrared radiative properties and forcing of cirrus. J Geophys Res 2007;112:D08201.
[7] Wylie DP, Menzel WP, Woolf HM, Strabala KI. Four years of global cirrus cloud statistics using HIRS. J Clim 1994;7:1972–86.
[8] Nazaryan H, McCormick MP, Menzel WP. Global characterization of cirrus clouds using CALIPSO data. J Geophys Res 2009;113:D16211.
[9] Mishchenko MI, Macke A. How big should hexagonal ice crystals be to produce halos? Appl Opt 1999;38:1626–9.
[10] Noel V, Winker DM, McGill M, Lawson P. Classification of particle shapes from lidar depolarization ratio in convective ice clouds compared to in situ observations during CRYSTAL-FACE. J Geophys Res 2004;109:2156–202.
[11] Ulanowski Z, Kaye PH, Hirst E, Greenaway R. Light scattering by ice particles in the Earth's atmosphere and related laboratory measurements. In: Proceedings of the electromagnetic light scattering conference XII; 2010.
[12] Cole BH, Yang P, Baum BA, Riedi J, Labonnote LC. Ice particle habit and surface roughness derived from PARASOL polarization measurements. Atmos Chem Phys 2014;14:3739–50.
[13] Liu C, Panetta RL, Yang P. The effective equivalence of geometric irregularity and surface roughness in determining particle single-scattering properties. Opt Soc Am 2014;22:23620–7.
[14] Ulanowski Z, Hesse E, Kaye PH, Baran AJ. Light scattering by complex ice-analogue crystals. J Quant Spect Rad Trans 2006;100:382–92.
[15] Connolly PJ, Flynn MJ, Ulanowski Z, Choularton TW, Gallagher MW, Bower KN. Calibration of the cloud particle imager probes using calibration beads and ice crystal analogs: the depth of field. J Atmos Ocean Tech 2007;24:1860–79.
[16] Pfalzgraff WC, Hulscher RM, Neshyba SP. Scanning electron microscopy and molecular dynamics of surfaces of growing and ablating hexagonal ice crystals. Atmos Chem Phys 2010;10:2927–35.
[17] Ritter G. The growth and morphology of small ice crystals in a diffusion chamber [PhD Thesis]. Hatfield, UK: University of Hertfordshire; 2015 Available at: http://uhra.herts.ac.uk/handle/2299/16329.
[18] Neshyba SP, Lower B, Benning M, Lawson A, Rowe PM. Roughness metrics of prismatic facets of ice. J Geophys Res Atmos 2013;118:3309–18.
[19] Wagner R, Linke C, Naumann K-H, Schnaiter M, Vragel M, Gangl M, Horvath H. A review of optical measurements at the aerosol and cloud chamber AIDA. J Quant Spect Rad Trans 2009;110:930–49.
[20] Kemppinen O, Nousiainen T, Lindqvist H. The impact of surface roughness on scattering by realistically shaped wavelength-scale dust particles. J Quant Spect Rad Trans 2015;150:55–67.
[21] Macke A, Mueller J, Raschke E. Single scattering properties of atmospheric ice crystals. J Atmos Sci 1996;53:2813–25.
[22] Liu C, Panetta RL, Yang P. The effects of surface roughness on the scattering properties of hexagonal columns with sizes from the Rayleigh to the geometric optics regimes. J Quant Spect Rad Trans 2013;129:169–85.
[23] Ulanowski Z, Kaye PH, Hirst E, Greenaway RS, Cotton RJ, Hesse E, Collier CT. Incidence of rough and irregular atmospheric ice particles from Small Ice Detector 3 measurements. Atmos Chem Phys 2014;14:1649–62.
[24] Yurkin MA, Hoekstra AG. The discrete-dipole-approximation code ADDA: capabilities and known limitations. J Quant Spect Rad Trans 2011;112:2234–47.
[25] Muinonen K, Saarinen K. Ray optics approximation for Gaussian random cylinders. J Quant Spect Rad Trans 2000;64:201–18.
[26] Muinonen K, Nousiainen T, Fast P, Lumme K, Peltoniemi JI. Light scattering by Gaussian random particles: ray optics approximation. J Quant Spect Rad Trans 1996;55:577–601.
[27] McCall DS. Measurement and modelling of light scattering by small to medium size parameter airborne particles.PhD thesis. Hatfield, UK: University of Hertfordshire; 2010 Available at: http://uhra.herts.ac.uk/handle/2299/6374.
[28] Jämsä S, Peltoniemi JI, Lumme K. Thermal emission from a rough surface: ray optics approach. Astron Astrophys 1993;271:319–25.
[29] Zhou C, Yang P. Backscattering peak of ice cloud particles. Opt Express 2015;23(9):11995–2003.

[30] Schmidt K, Yurkin MA, Kahnert M. A case study on the reciprocity in light scattering computations. Opt Express 2012;20:23253–74.
[31] Hesse E, Collier CT, Penttilä A, Nousiainen T, Ulanowski Z, Kaye PH. Modelling light scattering by absorbing smooth and slightly rough facetted particles. J Quant Spect Rad Trans 2015;157:71–80.
[32] Taylor L, Hesse E, Ulanowski Z, Kaye PH, Penttilä A, Nousiainen T. Beam tracing with diffraction. In: Proceedings of the 15th electromagnetic and light scattering conference: Leipzig, Germany; 21–26 June, 2015.
[33] Takano Y, Liou KN. Solar radiative transfer in cirrus clouds. Part 1: single scattering and optical properties of hexagonal ice crystals. J Atmos Sci 1989;46:3–19.
[34] Ulanowski Z, Hirst E, Kaye PH, Greenaway R. Retrieving the size of particles with rough and complex surfaces from two-dimensional scattering patterns. J Quant Spect Rad Trans 2012;113:2457–64.
[35] Borovoi A, Kustova N, Cole B. Interference phenomena at backscattering by ice crystals of cirrus clouds. Opt Express 2015;23:24557–71.
[36] Takano Y, Jayaweera K. Scattering phase matrix for hexagonal ice crystals computed from ray optics. Appl Opt 1985;24:3254–63.
[37] Yang P, Bi L, Baum BA, Liou KN, Kattawar GW, Mishchenko MI, Cole B. Spectrally consistent scattering, absorption, and polarization properties of atmospheric ice crystals at wavelengths from 0.2 to 100 μm. J Atmos Sci 2013;70:330–47.
[38] Ulaby FT, Moore RK, Fung AK. Microwave Remote Sensing: Active and Passive, Volume II. Mass., USA: Addison-Wesley Publ.; 1982.